JOURNAL OF AIRCRAFT
Vol. 42, No. 3, May–June 2005

Numerical Heat Transfer Correlation for Array of Hot-Air Jets Impinging on 3-Dimensional Concave Surface

Mathieu Fregeau,* F. Saeed,† and I. Paraschivoiu‡
École Polytechnique de Montréal, Montreal, Québec H3C 3A7, Canada

Numerical heat transfer correlations established from a numerical computational fluid dynamics (CFD) study of a three-dimensional hot-air jet array impinging on curved (circular) surface are presented. The results are in the form of numerical correlations for the average and maximum Nusselt number for different nozzle-to-nozzle spacing, nozzle-to-surface height, and hot-air jet Mach numbers typical of those in an hot-air antiicing system employed on aircraft wings. A validation case is presented, and it is shown that the results obtained from the CFD study are in good agreement with experimental data found in the literature. An interpolation technique, the Dual-Kriging method, that makes use of the numerical database for antiicing simulation on aircraft wings is presented. The benefit of using the Dual-Kriging method is that it preserves the nonlinear nature of the heat transfer distribution from a hot-air jet impinging on a curved surface.

Nomenclature

a_i	=	derivative function coefficient
C_p	=	specific heat at constant pressure
$c_1, \ldots, c_8$	=	correlation coefficient
d	=	piccolo hole (jet) diameter
G	=	mass flow rate of air per unit area, $\dot{m}/S$
H	=	nozzle-to-surface distance
h	=	Euclidean's distance
h_{av}	=	average heat transfer coefficient
h_c	=	heat transfer coefficient
I	=	identity matrix
K	=	generalized covariance term
k	=	thermal conductivity
M	=	Mach number
$\dot{m}$	=	mass flow rate of air, $\rho_{\text{jet}} A_{\text{noz}} V_{\text{jet}}$
N	=	number of variables
Nu	=	Nusselt number based on jet diameter, $h_c d/k$
n	=	number of samples per variable
Pr	=	Prandlt number, $C_p \mu/k$
$\dot{q}$	=	heat flux
Re	=	Reynolds number, $V_{\text{jet}} d/\nu$
S	=	reference surface area
s	=	coordinate along surface with origin at center of jet axis, $y = 0$ plane
T	=	temperature, K
U	=	general function
V_{jet}	=	mean jet velocity at exit of piccolo tube
W	=	nozzle-to-nozzle distance
X	=	multivariable sampling
x	=	one variable sampling
x, y, z	=	coordinate system with origin at center of jet exit
Γ	=	Kriging matrix
$\hat{\Gamma}$	=	weighted Kriging matrix
μ	=	dynamic viscosity
ν	=	kinematic viscosity, μ/ρ
ρ	=	fluid density
σ	=	weight value
Φ	=	derivative function
Ψ	=	covariance function

Subscripts

anti	=	from the antiicing system
jet	=	at the exit of piccolo tube (jet condition)
max	=	at the maximum point of the indexed variable
s	=	at the surface

Superscript

$\sim$	=	interpolated function or variables from which interpolations are made

Introduction

AN icing condition is a real potential hazard during climb and descent of aircraft. Because the aerodynamics performance is seriously altered when ice accretes on wings, stalling or losing command of control surface can cause serious safety deficiencies. To enhance flight safety under natural icing conditions, one of the several key tasks outlined in the Federal Aviation Administration (FAA) In-Flight Aircraft Icing Plan is to ensure the validity and reliability of icing simulation and modeling methods currently being used and developed.[1,2] In an effort to support the objectives of the FAA icing plan, and facilitate Bombardier Aerospace in the certification process, the main focus of research under the J.-A. Bombardier Aeronautical Chair at École Polytechnique, Montreal, has been the development of a reliable ice accretion and antiicing simulation code CANICE.[3–8] The development of CANICE has been geared toward the specific needs of Bombardier Aerospace. The antiicing simulation is commonly used on the Bombardier Aerospace regional jets, hot-air antiicing system. The antiicing system uses hot air from the engine compressor bleed. A system of external mounted ice detectors with a sensing probe oscillating with a set frequency that decreases as ice accumulates on the surface act as a warning system.

The focus of the present study is on the heat transfer distribution on the leading-edge internal surface when the antiicing system is used, that is, an array of round hot-air and high-speed jets. A review of the literature reveals that only few experimental and theoretical/numerical studies have been carried out to study the heat transfer and flow in the internal hot-air region.[9–13] These studies have focused on specific concerns that neither address the issues

Presented as Paper 2003-3403 at the 21st Applied Aerodynamics Conference, Orlando, FL, 23–26 June 2003; received 30 July 2003; revision received 20 May 2004; accepted for publication 28 July 2004.

*Graduate Research Student, Department of Mechanical Engineering, P.O. Box 6079, Succ. Centre-Ville.

†Research Associate, Department of Mechanical Engineering, P.O. Box 6079, Succ. Centre-Ville; currently Assistant Professor, King Fahd University of Petroleum and Minerals, Mail Box 1637, Dhahran 31261, Saudi Arabia. Member AIAA.

‡Bombardier Aeronautical Chair Professor, Department of Mechanical Engineering, P.O. Box 6079, Succ. Centre-Ville.

related to the design of a hot-air anti-icing system nor highlight variables that might play an important part in an optimum design of such a system. A numerical model using flat plate as impingement surface has previously been implemented into CANICE code and has shown lack of accuracy in heat transfer far from impingement point.[10,14] Hence, the need for an in-depth analysis of a hot-air antiicing system is significant.

Numerical simulation using computational fluid dynamics (CFD) has become a reliable tool to fill the gap left by a lack of experimental data. Therefore, this study was conducted using state-of-the-art commercial CFD software, FLUENT. The main goal was to use CFD to determine the local Nusselt number distribution on a concave surface from an array of hot-air jets. The local Nusselt number distribution $Nu(s, y)$ is determined for various values of Mach number, nozzle-to-surface height, and nozzle-to-nozzle spacing, for the particular case of a singular array of round-shaped nozzles. On the basis of the numerical prediction, a correlation is established to interpolate the local Nusselt number, the average Nusselt number Nu_{av}, and the maximum Nusselt number $Nu_{\max}$ within the range of the domain of study.

A previous study presents all of the details about the numerical simulation modeling and results.[15] Some brief details of the CFD modeling, results, and a validation case will, however, be reviewed for comprehension.

An exponential-based numerical correlation will be derived from the parametrized variables. The Kriging interpolation technique is being used for implementation in the CANICE-3D antiicing module and will be described. Results of the Kriging interpolation implementation will be presented and discussed.

Numerical Study

For a generic single array of round hot-air jets impinging on a curved surface, the local Nusselt number distribution can be expressed as

$$Nu = f[(s/d), (y/d), M_{\text{jet}}, (H/d), (W/d)] \tag{1}$$

When a constant temperature of 400 K for the hot-air jet and a circular-shaped impingement surface are considered, the distance H is used as the nozzle-to-surface distance as well as the radius of the arc of the curved surface. Although the leading-edge profile of an aircraft wing is not a perfect circular shape, the use of a circular profile is by far the best model that can be used for parametric representation and analytical model. In addition, a single array and a constant nozzle diameter of 2.5 mm were selected. The temperature on the impingement surface was kept constant at 260 K. Figure 1 shows the coordinate reference frame used and Fig. 2 the geometric parameters used for the antiicing model.

Nine different geometric configurations have been simulated at three different jet Mach number conditions. All cases examined in the study are listed in Table 1.

The numerical simulation of the three-dimensional internal hot-air flow has been conducted using the commercial CFD package

Table 1 Geometric characteristics and operating conditions

Variables	Values		
Jet Mach number M_{jet}	0.4	0.6	0.8
Height-to-diameter ratio H/d	5	10	15
Jet spacing-to-diameter ratio W/d	7.5	15	22.5

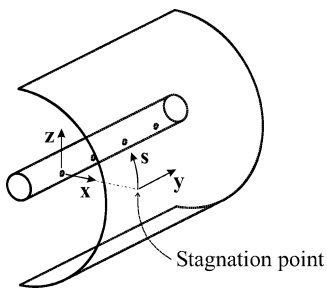

Fig. 1 Coordinate system used for antiicing system modeling.

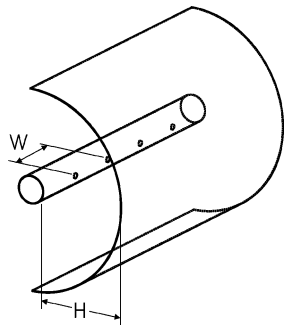

Fig. 2 Geometric parameters.

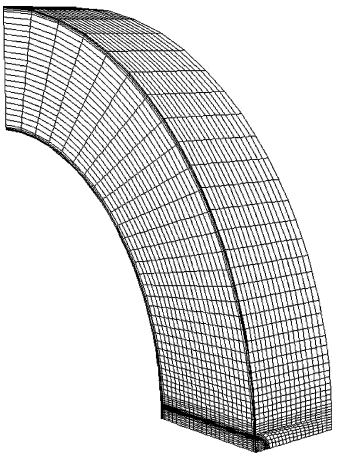

Fig. 3 Structured mesh used.

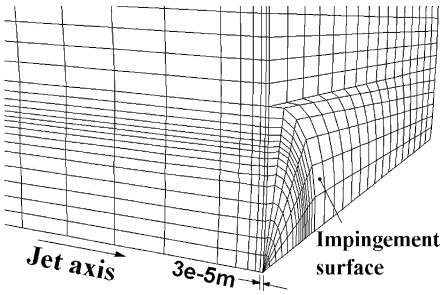

Fig. 4 Mesh concentration near impact surface, exterior view.

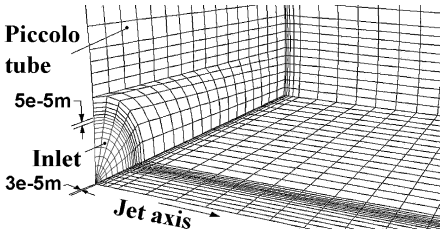

Fig. 5 Mesh concentration near inlet, interior view.

FLUENT (version 6.0.20). The FLUENT code can simulate a large variety of flow problems from subsonic to hypersonic viscous and inviscid conditions. Many of the turbulent models are encoded with some variable coefficients and wall laws; however, you can add your own function that rules most variables.[16]

Because the high compressibility of the flow and high Reynolds number imply region of high-velocity gradients, the Spalart–Allmaras turbulence model was used. This single, vorticity-based turbulence equation model keeps the resolution at a low level of complexity. In all cases, the boundary-layer mesh was kept constant to ensure a y^+ below 1. Figure 3 shows a typical mesh. There was a concentration near the exit of the piccolo hole as well as near the impingement region. First cell height was 0.00003 in those regions, as shown in Figs. 4 and 5.

Table 2 Operating conditions used for validation

Variable	Value
Jet Mach number M_{jet}	0.4
Jet height-to-diameter ratio H/d	6
Jet spacing-to-diameter ratio W/d	20.0
Hole diameter d	6.35 mm
ΔT $(T_{\text{jet}} - T_s)$	20 K

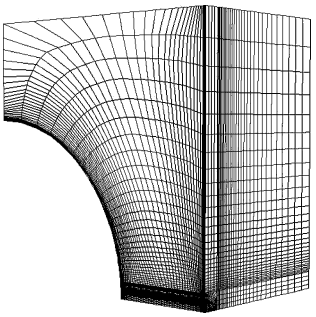

Fig. 6 Mesh used for validation case.

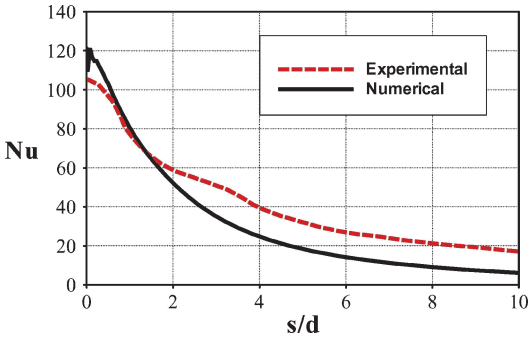

Fig. 7 Heat transfer distribution from jets impinging on a flat plate.

Validation Case

To establish the validity of our CFD model, the Gardon and Cobonpue study has been used for comparison.[17] This experimental study uses a flat plate as the impingement surface. A similar numerical three-dimensional model of the linear array of jets impinging on a flat plate was examined. A summary of the input conditions for the validation case is in Table 2. The boundary-layer mesh near the exit hole has been set to ensure a $y^+_{\max}$ below 1 on all surfaces. Figure 6 shows the mesh used for the validation case.

The local Nusselt number distribution across the surface was determined numerically and is plotted in Fig. 7 along the surface length axis with the empirical results of Gardon and Cobonpue.[17] As evident from Fig. 7, the predicted local Nusselt number distribution shows good agreement with empirical distributions. The first 5% of s/d shows higher heat transfer in the numerical results, which can be attributed to the use of a first-order spatial discretization scheme.[15] The next 5–20% of the s/d range shows sharp agreement, whereas the remaining 80% shows an increase in the error, with a continuous lower local Nusselt for the numerical part. Using a rectangular-shaped array for the experimental study instead of a linear array would suggest less energy dissipation far from the stagnation point for the experimental part.

Numerical Correlation

The averaged heat transfer coefficient per unit area h_{av} is retrieved by integrating the local heat transfer coefficient over a reference surface S divided by this reference surface area, as

$$\overline{h_c} = \frac{1}{S}\oint_S h_c \, \mathrm{d}s \tag{2}$$

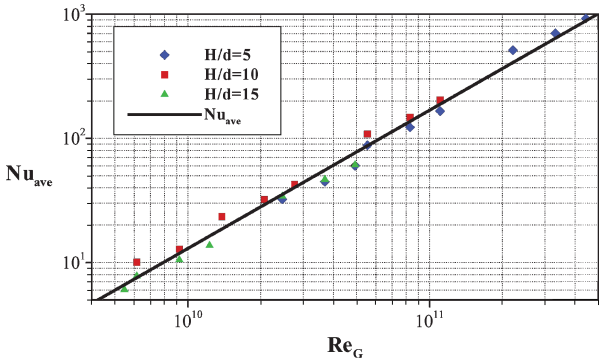

Fig. 8 Correlation of Nusselt number $\bar{N}u$ against Reynolds number Re_G.

where

$$S = (\pi/2)(HW)(H/d)(W/d)^{\frac{3}{2}} \tag{3}$$

The averaged Nusselt number Nu_{av} related to the mass-flow Reynolds number Re_G presents a correlation factor $R^2 = 0.9901$, using a power-law least-squares technique,

$$\overline{Nu} = 10^{-10} Re_G{}^{1.1131} \tag{4}$$

where

$$\overline{Nu} = \overline{h_c} H/k \tag{5}$$

The Reynolds number Re_G considers the mass flow per unit area and the parameter H,

$$Re_G = G/d\mu HW \tag{6}$$

$$G = \dot{m}/S \tag{7}$$

Correlation is shown in Fig. 8.

Correlation (4) shows a strong dependance of nozzle-to-surface distance H on the averaged Nusselt number.

Furthermore, by studying maximum Nusselt number, we established an exponential-based correlation by considering all variables in the general form of

$$Nu_{\max} = c_1 M^{c_2} (H/d)^{c_3} (W/d)^{c_4} \exp[c_5 (H/d)^{c_6} (W/d)^{c_7}] + c_8 \tag{8}$$

When a multivariate optimization process to minimize standard deviation from the numerical data, coefficients are determined resulting in

$$Nu_{\max} = 0.282 M^{0.49} (H/d)^{-1.69} (W/d)^{-0.856} \exp[9.14 (H/d)^{0.034} (W/d)^{0.074}] - 3 \tag{9}$$

Correlation (9) shows that nozzle-to-nozzle spacing has a negligible effect on the maximum Nusselt number. Indeed, regardless of the nozzle-to-nozzle distance, Nusselt number $Nu_{\max}$ is found at the stagnation point. Nusselt number $Nu_{\max}$ reflects a strong dependance on jet Mach number.

Kriging Interpolation

To avoid handling numerous data to establish correlation, we use a Kriging method. Even though there are many Kriging techniques to interpolate data, the focus of this study is on Dual Kriging.[18,19] Dual Kriging consists of establishing a derivative function, for example $\Phi(X)$, and a fluctuation or covariance function, for example $\Psi(X)$. The interpolated function U on the domain X is then represented by

$$U(X) = \Phi(X) + \Psi(X) \tag{10}$$

Table 3 Common derivative forms for Dual Kriging

Derivative	Form
Constant	$\Phi(X) = a_0$
Linear	$\Phi(X) = a_0 + a_1 x_I + a_2 x_{II} + \cdots + a_N x_N$
Quadratic	$\Phi(X) = a_0 + a_1 x_I + \cdots + a_N x_N + a_{N+1} x_I^2$ $+ \cdots + a_{2N} x_N^2 + a_{2N+1} x_I x_{II}$ $+ \cdots + a_{2N+N-1} x_I x_N$ $+ \cdots + a_{2N+N^2-N} x_N x_{N-1}$
Trigonometric	$\Phi(X) = a_0 + a_1 \cos(\omega x_I)$ $+ \cdots + a_N \cos(\omega x_N) + a_{N+1} \sin(\omega x_I)$ $+ \cdots + a_{2N} \sin(\omega x_N)$

Table 4 Common covariance forms for Dual Kriging

Covariance	Form
Linear	$K(h) = h$
Cubic	$K(h) = h^3$
Logarithmic	$K(h) = h^2 \ell_n(h)$
Trigonometric	$K(h) = \sin(\omega h)$

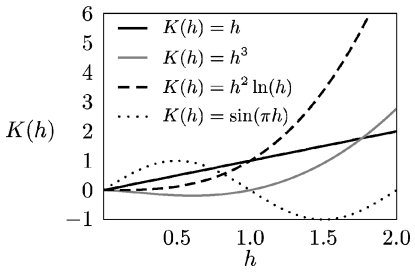

Fig. 9 Effect on *K* using different covariance function.

The domain on which we interpolate can be of the form of a one-dimensional vector, containing several data points, as well as a multi-dimensional matrix, for multivariate analysis, as

$$X = [x_I \quad x_{II} \quad x_{III} \quad \ldots] \tag{11}$$

where

$$x_I = [x_{I_1} \quad x_{I_2} \quad \ldots \quad x_{I_n}]^T \tag{12}$$

where variable x_I stands for the vector containing the data points for a specific variable, from a least-square point of view, the derivative function stands for the mean value of the function. Although the covariance function lets the Kriging function pass through all sample data points, the derivative function is imperative because it retains the behavior of the data. Most common derivative functions are summarized in Table 3. Typically, a constant or linear derivative function is sufficient when the function steadily evolves and does not show sparse discontinuities.

The covariance function reduces locally the standard deviation of interpolated function. A proper covariance function will make the interpolation scheme pass through all points by correcting the derivative function. When use is made of a normalized Euclidean distance h in the covariance function, the derivative function effect can be segregated. Table 4 summarizes most common covariance forms. Linear, cubic, and logarithmic covariance forms behave similarly to one-, two-, and three-dimensional spline-type interpolation. However, the logarithmic covariance form is best suited for multidimensional problems.[18] Other covariance forms could be developed as generic forms and could be more suited in the case of very sparse sampling. Equations (15) and (16) show other examples of covariance terms. Figure 9 shows the effect of different covariance function on the generalized covariance term K. Thus,

$$\Psi(X) = \sum_{i=1}^{n} b_i K(h_i) \tag{13}$$

where

$$h_i = |x - x_i| \tag{14}$$

$$K(h) = h^{2p+1} \tag{15}$$

$$K(h) = h^{2p} \ell_n(h) \tag{16}$$

The Dual-Kriging problem take the form of a linear system from which we compute the coefficients a and b of the derivative and covariance functions. In the case of sparse measurements or to avoid the effect of a misleading point, or noise, we can add a weight term to the generalized covariance term K by multiplying the Kriging matrix by a weight factor σ, as

$$\hat{\Gamma} = \Gamma + \sigma I \tag{17}$$

with

$$0 \le \sigma < h_{\max} \tag{18}$$

The weight term tends to smooth the interpolation scheme, converting the problem to a data-fitting scheme, avoiding an explicit fit through all sample points.

Having a linear derivative and a logarithmic covariance, the problem takes the form

$$\tilde{U} = a_0 + \begin{bmatrix} a_1 \\ a_2 \\ a_3 \\ a_4 \\ a_5 \end{bmatrix} \tilde{X} + \sum_{i=1}^{n} b_i K(|\tilde{X} - X_i|) \tag{19}$$

Normalizing parameter vectors by their respective maxima before the evaluation of the Euclidean's distance h ensures a good conditioning of the Kriging matrix Γ or $\hat{\Gamma}$.

Implementation of Dual-Kriging

We make use of the Dual Kriging to predict heat distribution from an array of hot-air jets impinging over a curved surface, taking into account the five parameters and data from the numerical study.

When use is made of a linear derivative and a logarithmic covariance, the Dual-Kriging linear system takes the form

$$\Gamma \boldsymbol{x} = \boldsymbol{f} \tag{20}$$

where

$$\boldsymbol{x} = \begin{bmatrix} b_1 \\ \vdots \\ b_n \\ a_0 \\ \vdots \\ a_N \end{bmatrix}, \qquad \boldsymbol{f} = \begin{bmatrix} Nu(X_1) \\ \vdots \\ Nu(X_n) \\ 0 \\ \vdots \\ 0 \end{bmatrix} \tag{21}$$

$$\Gamma = \begin{bmatrix} K(h_{ij}) & \cdots & \cdots & 1 & s_1 & y_1 & M_1 & (H/d)_1 & (W/d)_1 \\ \cdots & \cdots & \cdots & \vdots & \vdots & \vdots & \vdots & \vdots & \vdots \\ \cdots & \cdots & \cdots & 1 & s_n & y_n & M_n & (H/d)_n & (W/d)_n \\ 1 & \cdots & 1 & & & & & & \\ s_1 & \cdots & s_n & & & & & & \\ y_1 & \cdots & y_n & & & & & & \\ M_1 & \cdots & M_n & & & & & 0 & \\ (H/d)_1 & \cdots & (H/d)_n & & & & & & \\ (W/d)_1 & \cdots & (W/d)_n & & & & & & \end{bmatrix} \tag{22}$$

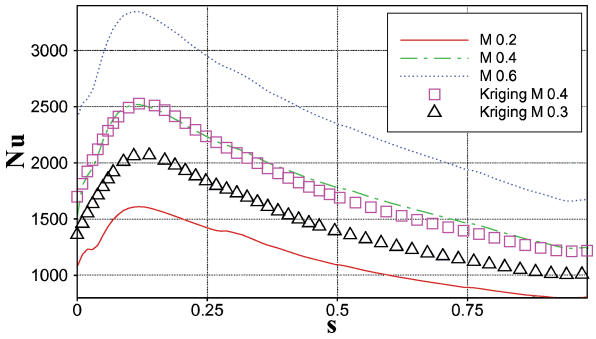

Fig. 10 Interpolation using Kriging technique within data of study.

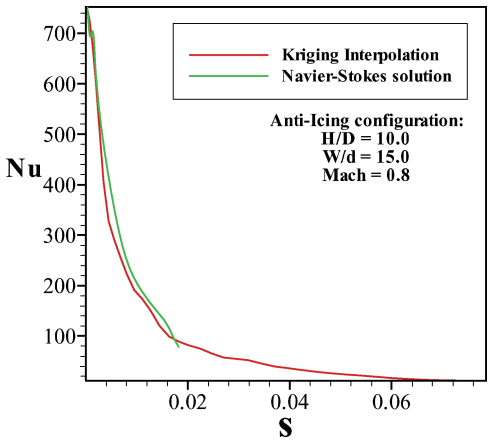

Fig. 11 Two-dimensional interpolation over NACA0015 leading edge using Kriging technique.

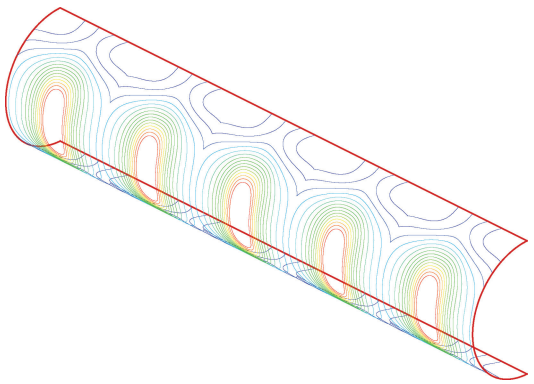

Fig. 12 Three-dimensional interpolation over NACA0015 leading edge using Kriging technique.

The domain used reflects the one used in the antiicing interpolation module. Figure 10 shows the use of the Kriging technique by taking three distributions of heat transfer over curve length s for different Mach numbers. An interpolated curve is calculated for $M = 0.4$ and shows excellent agreement with numerical data. A second interpolated curve is calculated to compute the $M = 0.3$ distribution line.

Having a NACA0015 as a two-dimensional profile from root to tip of a wing, we establish the closest circular shape that minimizes standard deviation over 15% of the chord. Then with a generic span of 1 m, an H/d of 10, a W/d of 15, and a jet Mach number of 0.8, we estimate a heat transfer distribution from the multidimensional Kriging method within the results from the numerical study. Figure 11 shows interpolated heat transfer from the antiicing configuration over the curve length s and Fig. 12 shows the interpolated heat transfer over the wing leading edge.

Conclusions

Results from a CFD investigation of heat transfer from an array of hot-air jets impinging on a three-dimensional concave (circular) surface were presented.

Correlations have been established for the averaged and maximum Nusselt numbers for different nozzle-to-nozzle spacing, nozzle-to-surface height, and hot-air jet Mach numbers configurations. Values taken for the numerical study are typical of those for hot-air jets based an antiicing system employed for an aircraft wing at Bombardier Aerospace.

A validation case shows good agreement with the experimental data found in the literature.

The Dual-Kriging interpolation technique has been implemented as a simulation tool for the antiicing simulation module of CANICE-3D. This scheme interpolates a heat transfer distribution from the CFD result database for a given antiicing configuration.

The Dual-Kriging method preserves the non-linear nature of the heat-transfer distribution from hot-air jets impinging over a curved surface and, thus, is a clever interpolation scheme for this problem.

Acknowledgments

The authors would like to acknowledge the support of Natural Sciences and Engineering Research Council of Canada through a cooperative R&D Grant. Bombardier Aerospace and the Advanced Aerodynamics Group are gratefully acknowledged for their helpful assistance. We would also like to thank King Fahd University of Petroleum and Minerals for its helpful support.

References

[1] *FAA International Conference on Aircraft In-Flight Icing*, Vols. 1 (A834613) and 2 (A144613), Federal Aviation Administration, Systems Resource Management Inc., Kensington, MD, 1996, pp. 6–8.

[2] "FAA In-Flight Icing Plan," Federal Aviation Administration, Technical Rept., U.S. Dept. of Transportation, April 1997.

[3] Morency, F., Tezok, F., and Paraschivoiu, I., "Antiicing System Simulation Using CANICE," *Journal of Aircraft*, Vol. 36, No. 6, 1999, pp. 999–1006.

[4] Morency, F., Tezok, F., and Paraschivoiu, I., "Heat and Mass Transfer in the Case of an Antiicing System Modelization, *Journal of Aircraft*, Vol. 37, No. 2, 2000, pp. 245–252.

[5] Tran, P., Brahimi, M. T., Sankar, L. N., and Paraschivoiu, I., "Ice Accretion Prediction on Single and Multi-Element Airfoils and the Resulting Performance Degradation," AIAA Paper 97-0178, Jan. 1997.

[6] Tran, P., Brahimi, M. T., Paraschivoiu, I., Pueyo, A., and Tezok, F., "Ice Accretion on Aircraft Wings with Thermodynamic Effects," *Journal of Aircraft*, Vol. 32, No. 2, 1995, pp. 444–446.

[7] Paraschivoiu, I., Tran, P., and Brahimi, M. T., "Prediction of the Ice Accretion with Viscous Effects on Aircraft Wings," *Journal of Aircraft*, Vol. 31, No. 4, 1994, pp. 855–861.

[8] Tran, P., Brahimi, M. T., and Paraschivoiu, I., "Ice Accretion on Aircraft Wings," *Canadian Aeronautics and Space Journal*, Vol. 40, No. 3, 1994, pp. 185–192.

[9] Martin, H., "Heat and Mass Transfer between Impinging Gas Jets and Solid Surfaces," *Advances in Heat Transfer*, Vol. 13, Academic Press, 1977, pp. 1–60.

[10] Saeed, F., Morency, F., and Paraschivoiu, I., "Numerical Simulation of a Hot-Air Anti-Icing Simulation," *38th Aerospace Sciences Meeting & Exhibit*, AIAA, Vol. 2, Reston, VA, 2000, pp. 897–904.

[11] Brown, J. M., Raghunathan, S., Watterson, J. K., Linton, A. J., and Riordon, D., "Heat Transfer Correlation for Anti-Icing Systems," *Journal of Aircraft*, Vol. 39, No. 1, 2002, pp. 897–904.

[12] Meola, C., Carlomagno, G. M., Riegel, E., and Salvato, F., "An Experimental Study of an Anti-Icing Hot Air Spray-Tube System," *Proceedings of the 19th Congress International Council of the Aeronautical Sciences*, Vol. 3, Paper No. 2345-2351, Sept. 1994.

[13]Croce, G., Habashi, W. G., Guevremont, G., and Tezok, F., "3D Thermal Analysis of an Anti-Icing Device Using FENSAP-ICE," AIAA Paper 98-0193, Jan. 1998.

[14]Saeed, F., and Paraschivoiu, I., "Numerical Correlation for Local Nusselt Number Distribution for Hot-Air Jet Impingement on Concave Surfaces," *Proceedings of the 8th Annual Conference of the CFD Society of Canada*, Ottawa, Vol. 2, 2000, pp. 897–904.

[15]Fregeau, M., Gabr, M., Saeed, F., and Paraschivoiu, I., "Numerical Simulation of Heat Transfer from an Array of Hot-Air Jets Impinging on a 3D Concave Surface," *Proceedings of the 50th CASI Annual General Meeting*, 2003; also *Canadian Aeronautical and Space Journal* (to be published).

[16]"Fluent 6.0 User's Guide," Fluent Company, Lebanon, NH, Dec. 2001.

[17]Gardon, R., and Cobonpue, J., "Heat Transfer Between a Flat Plate and Jets of Air Impinging on It," *International Developments in Heat Transfer*, ASME, New York, Pt. 2, 1961, pp. 454–460.

[18]Trochu, F., "Krigeage en CAO et FAO," MEC6310 Technical Rept. Ecole Polytechnique de Montréal, Montreal, QC, Canada, Sept. 2001.

[19]Cressie, N. A. C., *Statistics for Spatial Data*, Wiley, New York, 1993, Chap. 3.